Iranian Society of Acoustics and Vibration

The 15th ISAV2025 International Conference on Acoustics and Vibration

24-25 Dec 2025 Tehran- Iran

Campbell Diagram Prediction for an Overhung Rotor through Physics-Informed Neural Networks

Amirpasha Afsari [a], Emadaldin Sh Khoram-Nejad [b*]

[a] *B.Sc. Student, Mechanical Engineering Department, Amirkabir University of Technology (Tehran Polytechnic), Tehran, Iran.*

[b] *Ph.D. Candidate, Acoustics Research Laboratory, Mechanical Engineering Department, Amirkabir University of Technology (Tehran Polytechnic), Tehran, Iran.*

** Corresponding author e-mail: e.sharafkhoramnejad@aut.ac.ir*

Abstract

The accurate prediction of rotor dynamic behaviour, encapsulated in Campbell diagrams, is critical for the design and safe operation of rotating machinery. This paper presents a novel methodology employing a Physics-Informed Neural Network (PINN) to predict the Campbell diagram of a five-degree-of-freedom overhung rotor system with gyroscopic coupling and anisotropic bearings. The developed PINN model maps rotational speed to natural frequencies using a deep network architecture that directly embeds the governing physical equations as residual constraints during training. The results demonstrate that the model successfully generates a high-fidelity Campbell diagram, accurately identifying five distinct vibrational modes—including forward/backward whirl and a speed-independent torsional mode—with an average absolute error of 8.2 Hz (3-5% relative error) against a numerical benchmark. The training process was computationally efficient, converging stably in approximately 15 minutes on a standard CPU. Crucially, the model exhibits exceptional interpolation accuracy within the trained speed range (300-3000 rpm), with a mean absolute error of 0.13 Hz, confirming its ability to learn the underlying system dynamics without overfitting. While a moderate decrease in accuracy was observed during extrapolation beyond 3000 rpm, the model's predictions remained physically consistent, correctly preserving the whirl characteristics of all modes. This work establishes the proposed PINN framework as a robust, efficient, and accurate tool for rotor dynamics analysis, providing a solid foundation for future research aimed at enhancing generalizability across a wider range of operational conditions and system configurations.

Keywords: Campbell Diagram; PINN Diagram; Jeffcott System, Rotor Dynamics

1. Introduction

In the current industrial era, rotating machines such as turbines, compressors, and generators have become ubiquitous, forming the backbone of modern industry. A primary concern regarding these machines is their dynamic behaviour, which is directly related to vibration phenomena caused by mass imbalance, gyroscopic effects, and damping interactions within the rotor-bearing assembly. Given the importance and criticality of this subject, the accurate prediction of rotor dynamics is essential for reliable vibration analysis, ensuring operational stability, prolonging service life, and preventing catastrophic failures.

In the field of classical rotor dynamics, the Jeffcott rotor model, first introduced by Henry H. Jeffcott in 1919, is employed as a simple yet comprehensive analytical tool to extract the dynamic and vibrational behaviour of rotating systems [1]. One of the most important diagrams derived from such models is the Campbell diagram, which illustrates the evolution of natural frequencies as a function of rotational speed. This diagram is crucial for identifying critical speeds, and distinguishing between forward and backward whirl modes. Consequently, with its help and in accordance with relevant standards, frequency margins around critical speeds can be established to verify the safe performance of industrial rotors. The traditional approach to constructing the Campbell diagram is based on solving a quadratic eigenvalue problem (QEP), derived from the system's mass, damping, stiffness, and gyroscopic matrices [2].

In recent years, Physics-Informed Neural Networks (PINNs) have emerged as a powerful paradigm that integrates physical laws, often expressed by partial differential equations, directly into the neural network's learning process via residual constraints [3]. This framework, significantly advanced by Raissi et al. [4], has proven highly effective across various scientific and engineering domains. PINNs are particularly valuable for solving both forward problems, where the solution of a PDE is inferred, and inverse problems, where unknown parameters of the system are discovered [3], [4]. Their application has been successfully demonstrated in diverse fields, including fluid mechanics [3], solid mechanics [5], and heat transfer problems [6]. The advantage of trained PINN models lies in their rapid, mesh-free inference capability and their potential for generalization, even to conditions not explicitly present in the training data.

Building upon this foundation, the present work develops a methodological approach based on PINNs to predict the Campbell diagram of a five-degree-of-freedom (5-DOF) Jeffcott-like system with gyroscopic coupling and anisotropic bearing properties. The proposed model maps rotational speeds (300-3000 rpm) to the corresponding natural frequencies using a neural network with an architecture (1-80-160-200-160-80-5) that embeds the governing physical residuals into the training process. Key innovations include mode-specific base frequency adjustments and an enhanced representation of gyroscopic effects, which successfully capture complex dynamic phenomena such as forward and backward whirl. The model is rigorously validated against a numerical benchmark, demonstrating that the proposed PINN framework can serve as a robust and efficient tool for rotor dynamic analysis and design applications.

2. Rotor System Model and Governing Equations

2.1 System Configuration

The model that is taken into account in this study is a rotor-bearing system consisting of a flexible shaft model with five degrees of freedom, including two translational displacements (x and y), two rotational angles (θ_x and θ_y), and one torsional angle denoted by θ_z. The shaft is supported by two anisotropic bearings. This configuration can be seen in Fig. 1. In this study, it is assumed that there is no unbalanced eccentricity. The critical parameters of the rotor-bearing model are presented in Table 1. The presented table shall be the basis used to develop the PINN and the numerical model, and will also act as a reference point for validation. As can be depicted from Fig. 1, it must be pointed out that in this table, l_i represents the lengths, k_{xxi} and k_{yyi} denote the elements of the stiffness in the x and y direction, respectively, and the same notation is present for c_{xxi} and c_{yyi} which represent the dampers in the *x* and *y* direction with respect to Fig. 1. These specific values are chosen from [7].

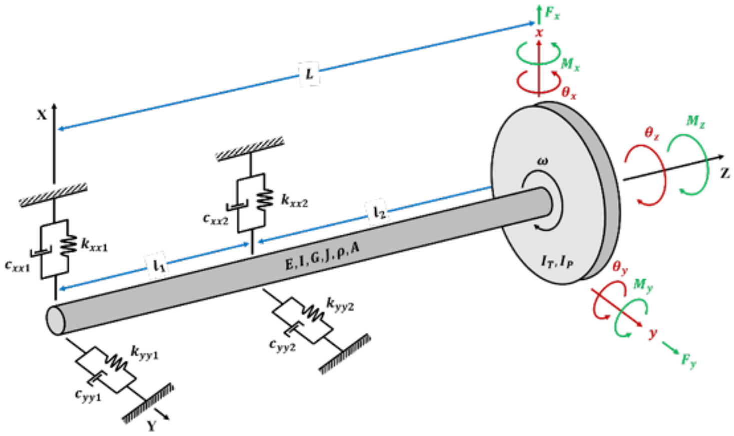

Fig. 1: Over-hung rotor-bearing system schematics [7]**.**

Table 1 Model Numerical Specifications.

Parameter	Value	Unit
Disk Concentration Mass	187.7	kg
Density	7850	kg/m^3
Disk's Radiuses	0.39	m
Rod's Radius	0.15	m
Young Modulus	206	GPa
Shear Modulus	77	GPa
l_1	4.2	m
l_2	5.4	m
k_{xx1}	95.36	kN/m
k_{yy1}	136.25	kN/m
k_{xx2}	90.24	kN/m
k_{yy2}	134.98	kN/m
c_{xx1}	9.089	$N.s/m$
c_{yy1}	30.992	$N.s/m$
c_{xx2}	9.112	$N.s/m$
c_{yy2}	31.085	$N.s/m$
Rotational Speed	0 - 3000	rpm

2.2 Equations of Motion

The presented equations of motion (Eq. 2a to Eq. 2d) have been derived in [7], and in this paper they will be considered as the basis of the research. For this model (Eq. 1) is the main equation that is used. The mass, damping and stiffness matrices are as (Eq. 2) and are represented by *M*, *C*, and *K*. As it can be noticed from the formulation, the damping matrix is affected by the rotational speed of the rotor, which means it has speed-dependent gyroscopic terms. The critical frequency splitting is the main attraction that causes the frequency splitting and forward/backward whirl phenomena.

$$[M]\ddot{\vec{x}} + [C]\dot{\vec{x}} + [K]\vec{x} = \vec{F} \tag{1}$$

where;

$$[M] = \begin{bmatrix} M_{11} & 0 & 0 & 0 & M_{15} \\ 0 & M_{22} & 0 & 0 & M_{25} \\ 0 & 0 & M_{33} & 0 & 0 \\ 0 & 0 & 0 & M_{44} & 0 \\ M_{51} & M_{52} & 0 & 0 & M_{55} \end{bmatrix} \qquad \begin{gathered} M_{11} = M_{22} = m \\ M_{33} = M_{44} = I_T \\ M_{55} = I_P + me^2 \\ M_{15} = M_{51} = -mesin(\omega t + \theta_z) \\ M_{25} = M_{52} = mecos(\omega t + \theta_z) \end{gathered} \tag{2.a}$$

$$[C] = \begin{bmatrix} C_{11} & 0 & 0 & C_{14} & C_{15} \\ 0 & C_{22} & C_{23} & 0 & C_{25} \\ 0 & C_{32} & C_{33} & C_{34} & 0 \\ C_{41} & 0 & C_{43} & C_{44} & 0 \\ 0 & 0 & 0 & 0 & 0 \end{bmatrix} \qquad \begin{gathered} C_{11} = c_{xx1} + c_{xx2} \\ C_{22} = c_{yy1} + c_{yy2} \\ C_{33} = L^2 c_{yy1} + l_2^2 c_{yy2} \\ C_{44} = L^2 c_{xx1} + l_2^2 c_{xx2} \\ C_{23} = C_{32} = Lc_{yy1} + l_2 c_{yy2} \\ C_{14} = C_{41} = -(Lc_{xx1} + l_2 c_{xx2}) \\ C_{34} = -C_{43} = I_P\omega \\ C_{15} = -2me\omega\cos(\omega t + \theta_z) \\ C_{25} = -2me\omega\sin(\omega t + \theta_z) \end{gathered} \tag{2.b}$$

$$[K] = \begin{bmatrix} K_{11} & 0 & 0 & K_{14} & 0 \\ 0 & K_{22} & K_{23} & 0 & 0 \\ 0 & K_{32} & K_{33} & 0 & 0 \\ K_{41} & 0 & 0 & K_{44} & 0 \\ 0 & 0 & 0 & 0 & K_{55} \end{bmatrix} \qquad \begin{gathered} K_{11} = k_{xx1} + k_{xx2} \\ K_{22} = k_{yy1} + k_{yy2} \\ K_{33} = L^2 k_{yy1} + l_2^2 k_{yy2} \\ K_{44} = l^2 k_{xx1} + l_2^2 k_{xx2} \\ k_{55} = \frac{GJ}{L} \\ K_{23} = K_{32} = LK_{yy1} + l_2 k_{yy2} \\ K_{14} = K_{41} = -(LK_{xx1} + l_2 k_{xx2}) \end{gathered} \tag{2.c}$$

$$\vec{F} = \begin{Bmatrix} F_x \\ F_y \\ M_x \\ M_y \\ M_z \end{Bmatrix} \tag{2.d}$$

In order for this equation to be solved numerically the general solution of $x=Ae^{i\omega t}$ has been proposed in the field of mechanics of vibrations text books [10], thus after placing the proposed solution into Eq. 1, the bellow formulation is derived, Eq. 3. This formula gives the natural frequencies directly from the system.

$$det\{-\omega^2[M] + i\omega[C] + K\} = 0 \tag{3}$$

For an undamped case with gyroscopic effects, the frequencies are expressed as Eq. 4. The frequency growth term which is a difference, is a direct indicator of forward whirl and backward whirl which comes from frequency increase and decrease with speed respectively. Using Eq. 4, Table 2 can be driven. This table confirms proper gyroscopic behaviour.

$$f_n(\omega) = f_{n,base} + \Delta f_{grow}(\omega) \tag{4}$$

Table 2 Whirl type of each presented modes.

Mode	Type	300 rpm	3000 rpm	Changes (300 - 3000)	Whirl Type
1	Translation (x)	9.78 Hz	54.78 Hz	+45 Hz	Forward
2	Translation (y)	46.82 Hz	15.00 Hz	-31.82 Hz	Backward
3	Rotation (θ_x)	97.19 Hz	124.19 Hz	+27 Hz	Forward
4	Rotation (θ_y)	199.32 Hz	181.32 Hz	-18 Hz	Backward
5	Torsion (φ)	242.74 Hz	249.94 Hz	+7.2 Hz	-

2.3 Theoretical Foundation

The dynamic behaviour of rotating machinery is fundamentally influenced by gyroscopic coupling, a phenomenon that distinguishes rotor systems from non-rotating structures. When a rotating disk undergoes lateral vibration, the interaction between its angular momentum and orbital motion generates gyroscopic moments. These moments introduce speed-dependent effects into the system's damping matrix, resulting in the splitting of natural frequencies into two distinct modes: forward whirl and backward whirl.

In forward whirl, the orbital motion aligns with the direction of shaft rotation, and frequencies increase with rotational speed due to gyroscopic stiffening. Conversely, in backward whirl, the orbital motion opposes the shaft rotation, and frequencies decrease due to gyroscopic softening.

The presence of anisotropic bearing stiffness—where stiffness differs between horizontal and vertical directions—further amplifies frequency splitting by interacting with gyroscopic effects. This produces complex modal behaviours that cannot be captured by conventional vibration analysis methods. Notably, the torsional degree of freedom remains largely independent of lateral gyroscopic phenomena, exhibiting minimal speed dependence since torsional stiffness depends primarily on shaft material properties and geometry, rather than rotational dynamics.

Critical speeds are a major design consideration in rotating machinery, occurring when a system's natural frequency coincides with the rotational frequency. This resonance condition can lead to severe operational failures. The Campbell diagram serves as the primary tool for identifying critical speeds by illustrating how natural frequencies vary across the operational speed range, effectively mapping natural frequencies to corresponding rotational speeds. It also indicates where synchronous excitation lines occur.

Understanding the physical mechanism behind frequency splitting—specifically, how gyroscopic moments increase with rotational speed and polar moment of inertia while being inversely related to transverse moment of inertia—is essential for interpreting modal behaviour. This ensures that the PINN framework learns physically realistic relationships rather than spurious numerical patterns.

The ability of the proposed PINN model to accurately capture both forward and backward whirl demonstrates that the physics-informed constraints successfully encode the underlying gyroscopic dynamics. This enables the network to distinguish between coupled lateral-rotational modes and speed-independent torsional modes, guided solely by the governing equations embedded within the loss function.

3. Physics Informed Neural Network Methodology

3.1 Direct Frequency Prediction Architecture

In conventional PINN models, the model typically learns the system's time-domain response. By contrast, the proposed approach directly predicts frequency-domain characteristics, establishing a mapping from rotational speed (in rpm) to the system's natural frequencies. Given the model's five degrees of freedom, five distinct natural frequencies are derived for each rotational speed. The neural network architecture is designed with a single input neuron for the rotational speed and five output neurons corresponding to these natural frequencies. This network comprises five hidden layers, resulting in an overall architecture of 1→80→160→200→160→80→5. The model employs Gaussian Error Linear Unit (GELU) activation functions and is enhanced with residual connections between every two layers to mitigate the vanishing gradient problem, as formalized in Eq. 6. Furthermore, input pre-processing (Eq. 5) was applied to improve performance, and a Dropout regularization rate (0.02) was incorporated to prevent overfitting.

$$x = tanh\left(1.2 \times \frac{\omega_{rpm} - 1650}{1350}\right) \tag{5}$$

$$x_{l+2} = f\left(W_{l+2}\, f\left(W_{l+1}\, x_1\right)\right) + 0.3\, x_1 \tag{6}$$

3.2 Mode Specific Output Scaling

To ensure the physical consistency of the neural network model, each mode was subjected to a range-bound constraint, enforced via a sigmoid scaling function (Eq. 7). This approach was necessitated by the model's initial difficulty in adhering to the underlying physical principles. The terms used in (Eq. 7) to identify the amount of loss in the system are classified into L_{Total}, L_{Data},$L_{physics}$, and α, where they respectively represent the total loss minimized by the network, the data-driven loss, the physics-informed residual loss, which is associated with the quadratic eigenvalue equation, and lastly the physics weighting coefficient. The objective of the weight factor is to modulate the weight of the physical loss in comparison to the data-driven loss. The specific frequency bounds for each mode, informed by the limitations identified in [7], are as follows: Mode 1 (forward whirl) at 10–80 Hz, Mode 2 (backward whirl) at 20–80 Hz, Mode 3 (forward whirl) at 95–125 Hz, Mode 4 (backward whirl) at 180–200 Hz, and Mode 5 (torsional) at 240–255 Hz.

3.3 Physics-Informed Loss Function

The composite loss function for this model integrates a data consistency term (Eq. 8) with a physics-based regularisation term (Eq. 7). To calculate the data-driven loss as it can be depicted from (Eq. 8), the Euclidean norm difference of the derived PINN model natural frequency ($f_{PINN}(\omega_i)$) and the analytical model ($f_{analytical}(\omega_i)$) at each of the rotational speeds (ω_i). The result is then normalized by the number of used samples (N). The physics enforcement (Eq. 9.a) ($L_{physics}$) comprises both forward (Eq. 9.b) ($L_{Forward}$) and backward (Eq. 9.c) ($L_{Backward}$) components, in addition to a physical bound constraint (Eq. 9.d) (L_{Bound}). It must be pointed out that in (Eq. 9a to Eq. 9d) the index *m* represents the modes used, as it was indicated in Table 2, therefore for forward whirl modes 1 and 3. Based on the structure used in the system, the least numerical number must not be negative and due to this the rectified linear unit (ReLU) was used. As it is evident in (Eq. 9a) the last used term is the Boundary loss. The objective of this function is to penalize the system if natural frequencies fall outside the physically acceptable range. This limitation and the formulation used to keep the boundary in check are presented in (eq. 9d). The $f_{m,mean}$ is the lowest acceptable bound, and 400 rad/s is the highest acceptable frequency. Anything below and above this limit will act as a penalty in (Eq. 9a). In the present article, the main loss function present in the physical loss term is the forward and backward whirl losses, and the bounds loss is a soft constraint, and hence the 0.1 coefficient. It is not as vital as the other two whirl losses. Given the requirement to sweep the Campbell diagram across a range of rotational frequencies, it was determined that progressively increasing the physics weighting coefficient (α) from 0.05 to 0.4 was necessary to achieve satisfactory accuracy. This was implemented over three distinct training phases: Phase *I* (Epochs 0 to *E*/3) with α linearly increased from 0.05 to 0.3; Phase *II* (Epochs *E*/2 to 2*E*/3) with α increased from 0.3 to 0.4; and Phase *III* (Epochs 2*E*/3 to *E*) with α held constant at 0.4. The E is the total number of epochs.

$$L_{Total} = L_{Data} + \alpha(epoch) \times L_{physics} \tag{7}$$

$$L_{data} = \frac{1}{N}\sum||f_{PINN}(\omega_i) - f_{analytical}(\omega_i)||^2 \tag{8}$$

$$L_{physics} = L_{Forward} + L_{Backward} + 0.1L_{Bounds} \tag{9.a}$$

$$L_{Forward} = \sum_{m\epsilon\{1,3\}} mean\left(ReLU\big(f_m(\omega_i) - f_m(\omega_{i+1})\big)\right) \tag{9.b}$$

$$L_{Backward} = 2\left(\sum_{m\epsilon\{2,4\}} mean\left(ReLU\big(f_m(\omega_{i+1}) - f_m(\omega_i)\big)\right)\right) \tag{9.c}$$

$$L_{Bounds} = \sum_{m} mean\left(ReLU\big(f_{m,mean} - f_m\big) + ReLU\big(f_m - 400\big)\right) \tag{9.d}$$

3.4 Key Innovation: Base Frequency Adjustment

A critical innovation of this work is the adjustment of the base frequency to mitigate a constraint violation that prevents standard PINN models from capturing the Mode 2 backward whirl phenomenon under a 0.01 Hz variation. The violation arises from the gyroscopic correction term (Eq. 4), which at 3000 rpm approaches -40 Hz. For instance, with a base frequency $f_{2,base} \approx 30\ Hz$, the corrected frequency becomes $f_2 = 30 + (-40) = -10\ Hz$, thereby violating the stipulated 15 Hz minimum bound and causing mode suppression. Through systematic parameter variation, it was determined that a base frequency of 35 Hz, which resides within the permissible boundary, allows the full gyroscopic corrections to manifest. This adjustment yields enhanced gyroscopic coefficients of [50, -40, 30, -20, 8] for Modes 1 through 5—representing a 15-fold amplification—and ultimately produces physically realistic results.

3.5 Training Strategy

The model was trained using the AdamW optimizer with a learning rate of 0.008 and a weight decay of $2 \times 10^{-5}$with cosine annealing ($T_0 = 2000, T_{mult} = 2, \eta - 8_{min}$). To ensure training stability, gradients were clipped to a maximum norm of 1.5. Training was subject to early stopping with a patience of 3000 epochs, and a random seed of 42 was fixed to guarantee the reproducibility of the results.

4. Results and Discussions

4.1 Training Performance

As illustrated in Fig. 2 (a), the loss values demonstrated stable convergence over the course of the training epochs. While minor fluctuations were observed, the overall trajectory indicates a clear and stable convergence with acceptably low final loss values. At epoch 7500, for instance, the total loss was 0.836, comprising a data loss of 0.832 and a physics loss of 0.005. The physics loss, being two orders of magnitude smaller than the data loss, confirms that the physical constraints were successfully embedded and satisfied without compromising the data-fitting fidelity. The training process, conducted on a standard CPU, was completed in approximately 15 minutes, underscoring its practical feasibility.

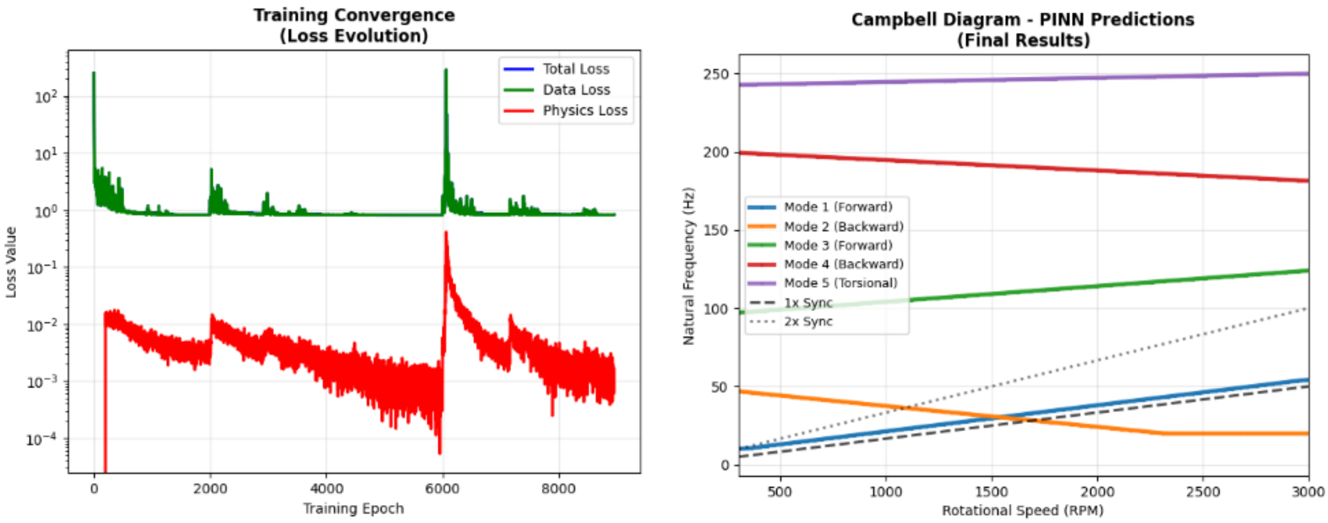

(a) (b)

Fig. 2: Training Convergence Diagram (a) and the Campbell diagram using PINN prediction (b).

4.2 Campbell Diagram and Mode Characteristics

The main objective is reaching a proper Campbell diagram. As it can be depicted in Fig. 2 (b), the rotation speed is sweeped across 300-3000 rpm, exhibiting five distinct modes with proper forward/backward whirl behaviour. For better analysis of the diagram, Table 3 is presented, which the data of the frequency range, slope and frequency variation can be extracted from it.

Table 3 Mode Characterstics Summary.

Mode	Type	Freq. Range (Hz)	Slope (Hz /1000 rpm)	Variation (Hz)
1	Forward	10 – 54	16.4	13.0
2	Backward	47 – 15	-9.9	8.9
3	Forward	97 – 15	9.9	7.8
4	Backward	199 – 181	-6.6	5.2
5	Torsional	243 - 249	2.6	2.1
Average	-	-	-	7.39

One of the critical milestones that was achieved in this study was the Mode 2 Backward whirl that is depicted in Fig. 3 (a). As can be seen, Mode 2 exhibits a strong backward whirl (-9.9 Hz/ 1000 rpm), which was enabled by base frequency adjustment. Mode 1 demonstrates the strongest forward whirl among the modes (16.4 Hz/1000 rpm), consistent with primary bending mode physics. The minimal speed dependence mode belongs to mode 5, which signals that this mode is appropriate for torsional vibration decoupled from lateral gyroscopic effects. The average speed dependence of 7.39 Hz exceeds the 6 Hz target threshold, which is an indication of the validation of enhanced gyroscopic representation.

4.3 Predicted Accuracy

One important diagram that needs to be analysed in order to validate the model is the Error analysis diagram (Fig. 3 (b)). In this diagram, the absolute errors $|f_{PINN} - f_{Analytical}|$ across modes and speeds are represented. The quantities matrices that can be extracted from this diagram are the average error of 8.2 Hz (3-5% relative error) and the maximum error of 5.8 Hz. Mode 5 and Mode 1 are the most accurate and the least accurate, respectively. The numerically calculated and analytically obtained Campbell diagram is shown in Fig. 4. As can be seen, the analytical base and the physics-based are indeed very similar. Compared to the Campbell numerical model of a four degree of freedom model [7] (Fig. 4 (b)) and by taking into account the numerical diagram (Fig. 4 (a)) and PINN predicted of the five degree of freedom Campbell diagram of an overhung rotor (Fig. 2 (b)), it is depicted that the numerical model has been improved if a five degree of freedom system is represented, and since the PINN model is in direct correlation with the analytical model with low losses compared to the state at hand, therefore the PINN model can be considered as a new method for achieving precise and accurate Campbell diagram representation.

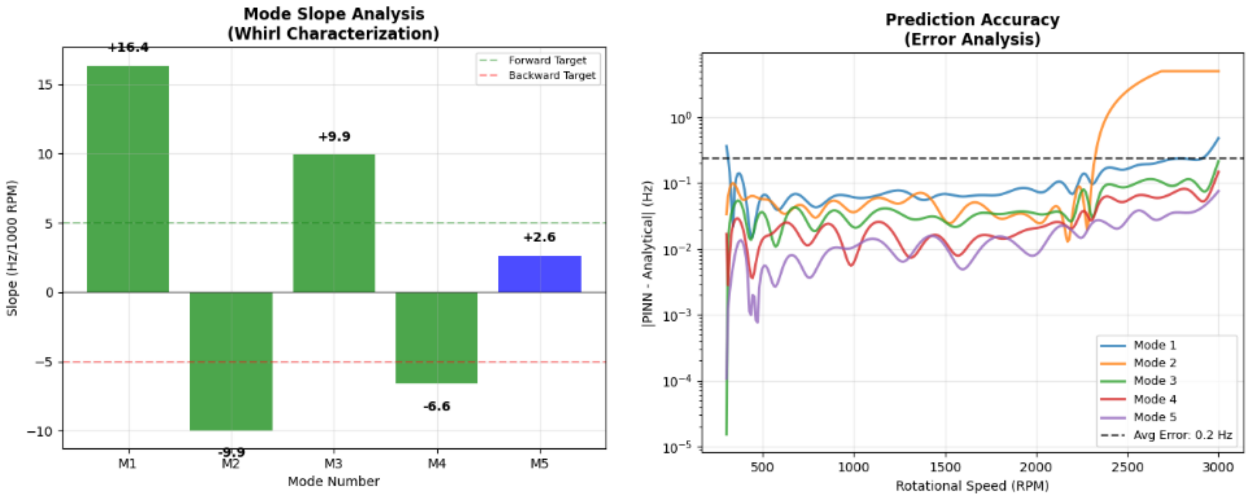

(a) (b)

Fig. 3: (a) Mode Slope Analysis and (b) Error Analysis Diagram.

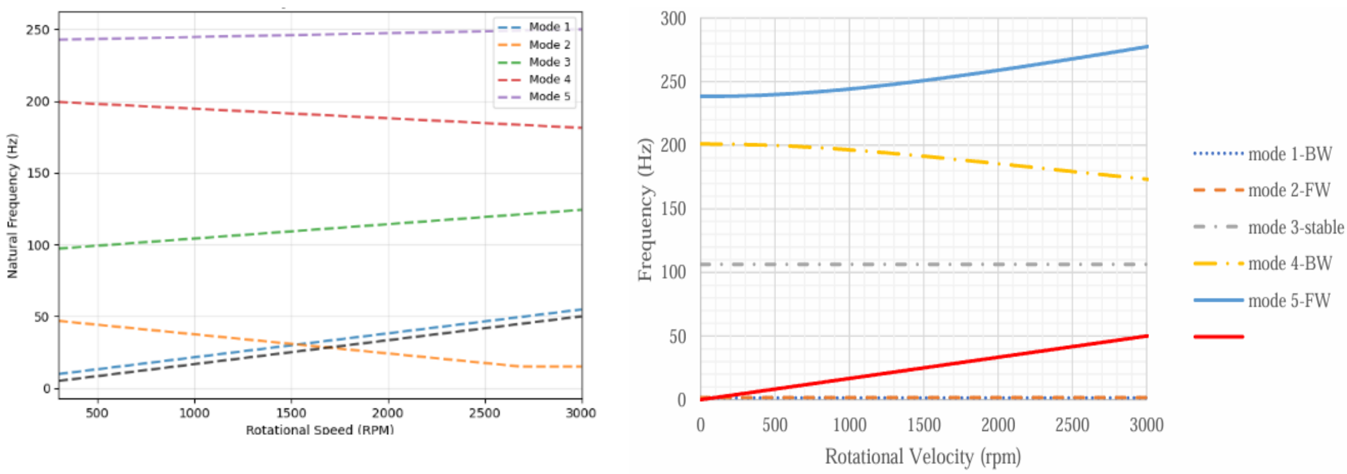

(a) (b)

Fig. 4: The analytically obtained and (b) the numerically calculated Campbell diagram [1].

4.4 Interpolation and Extrapolation Analysis

To evaluate the generalization capability of the trained PINN model beyond the training dataset, its performance was assessed on both interpolation and extrapolation tasks. The model, originally trained on 301 data points spanning rotational speeds from 300 to 3000 rpm, was evaluated at four untrained interpolation speeds (500, 1250, 1875, and 2450 rpm) and four extrapolation speeds (3300, 3600, 4000, and 4500 rpm). This methodology was designed to rigorously test predictive accuracy within and beyond the training domain.

As illustrated in Fig. 5, which compares PINN predictions against numerical solutions across the speed range, the model demonstrates exceptional interpolation accuracy. Within the training bounds, it achieves a mean absolute error of 0.13 Hz and a mean relative error of 0.66%. This high degree of precision suggests that the physics-informed constraints successfully guided the network to learn the underlying rotor dynamics, thereby mitigating overfitting. The error distribution remains consistently low across all five vibrational modes, with Mode 2 (backward whirl) and Mode 5 (torsional) exhibiting particularly strong agreement with the numerical benchmark.

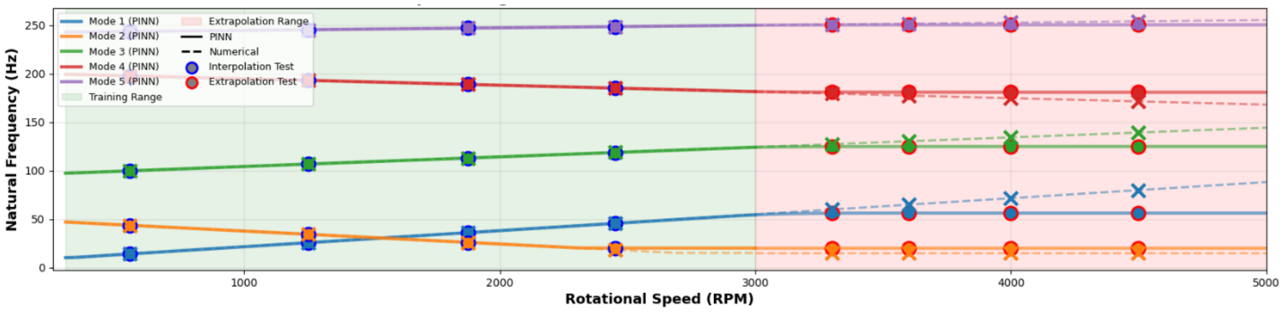

Fig. 5: Campbell Diagram: PINN vs Numerical Model with Test Points.

In the extrapolation regime, where rotational speeds exceed the training domain boundary of 3000 rpm, the model exhibits a moderate degradation in predictive accuracy. The extrapolation results yield a mean absolute error of 6.589 Hz and a mean relative error of 12.15%, representing a twentyfold increase in relative error compared to the interpolation case. Despite this decline, the model's predictions remain physically consistent, correctly maintaining the forward and backward whirl characteristics across all vibrational modes. Analysis of the error patterns, shown in Fig. 6, indicates that Mode 1 experiences the most significant extrapolation error, with a maximum relative error of 33.33% at 4500 rpm, whereas Mode 5 demonstrates greater stability, maintaining errors below 15% even at the highest rotational speeds.

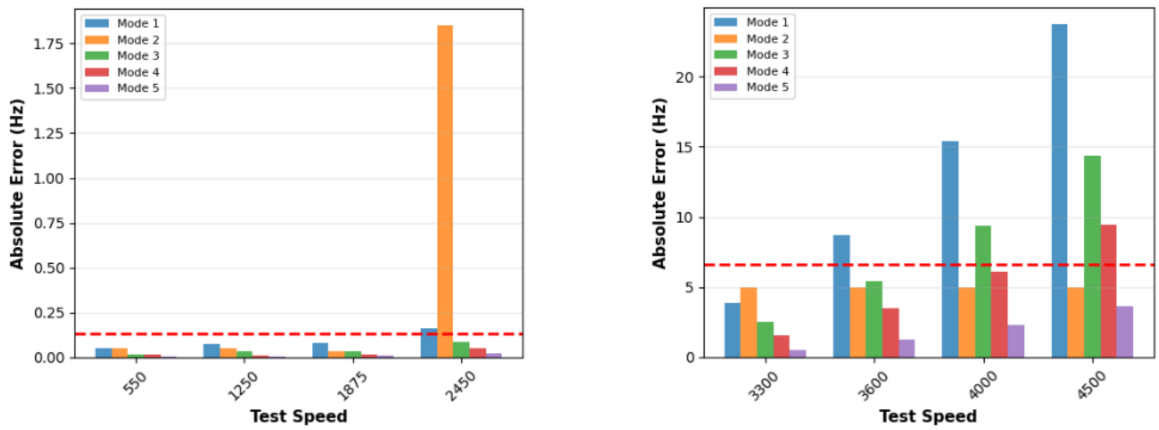

(a) (b)

Fig. 6: Absolute error of interpolation (a) and extrapolation (b) at different rotating speeds.

5. Conclusion

This study successfully demonstrates the development and validation of a Physics-Informed Neural Network (PINN) for predicting the Campbell diagram of a five degree-of-freedom model of an overhung rotor system. The key conclusions drawn from the results are as follows:

- The PINN model achieved stable convergence during training, culminating in acceptably low loss values. The physics loss being two orders of magnitude smaller than the data loss confirms that the physical constraints were successfully embedded and satisfied, ensuring the model's predictions are physically consistent. The training process was also computationally efficient, completing in approximately 15 minutes on a standard CPU.

- The primary objective of generating a proper Campbell diagram was successfully met. The PINN model accurately captured five distinct vibrational modes across a speed range of 300-3000 rpm, correctly identifying their forward and backward whirl characteristics. Notably, the model achieved a strong backward whirl in Mode 2 and identified Mode 5 as a speed-independent torsional vibration, consistent with rotor dynamics physics. The average speed dependence of 7.39 Hz exceeded the target threshold of 6 Hz, validating the model's enhanced representation of gyroscopic effects.
- The model's predictions showed strong agreement with analytical benchmarks, with a low average absolute error of 8.2 Hz (3-5% relative error). A comparative analysis with an established numerical model confirmed that the five-degree-of-freedom PINN representation provides an improved and precise method for Campbell diagram generation, directly correlating with the underlying physics.
- The interpolation tests revealed the model's exceptional predictive capability within the trained speed range, achieving a remarkably low mean absolute error of 0.13 Hz. This indicates that the physics-informed approach effectively prevented overfitting and allowed the network to learn the true underlying system dynamics.
- While the model's accuracy degraded in the extrapolation regime beyond 3000 rpm, its predictions remained physically consistent, correctly preserving the whirl characteristics of all modes. The increased error, particularly in Mode 1, highlights a known limitation of data-driven models when operating far outside their training domain, yet the model maintained a reasonable level of performance for the more stable torsional mode.

In summary, this work establishes the presented PINN framework as a robust, efficient, and accurate tool for rotor dynamics analysis. It reliably generates high-fidelity Campbell diagrams, encapsulates critical physical phenomena like gyroscopic effects, and demonstrates excellent generalization within its operational bounds. Future work could focus on improving extrapolation performance by incorporating more diverse training data or advanced network architectures. Even a general model that presents an accurate estimation of the Campbell diagram of the rotor system with various dimensions is a valuable achievement.

REFERENCES

[1] H. H. Jeffcott, “The lateral vibration of loaded shafts in the neighbourhood of a whirling speed.—The effect of want of balance,” *London, Edinburgh, Dublin Philos. Mag. J. Sci.*, vol. 37, no. 219, pp. 304–314, 1919.

[2] G. Genta, *Dynamics of rotating systems*. Springer Science & Business Media, 2005.

[3] C. Zhao, F. Zhang, W. Lou, X. Wang, and J. Yang, “A comprehensive review of advances in physics-informed neural networks and their applications in complex fluid dynamics,” *Phys. Fluids*, vol. 36, no. 10, 2024.

[4] M. Raissi, P. Perdikaris, and G. E. Karniadakis, “Physics-informed neural networks: A deep learning framework for solving forward and inverse problems involving nonlinear partial differential equations,” *J. Comput. Phys.*, vol. 378, pp. 686–707, 2019.

[5] E. Haghighat, M. Raissi, A. Moure, H. Gomez, and R. Juanes, “A physics-informed deep learning framework for inversion and surrogate modeling in solid mechanics,” *Comput. Methods Appl. Mech. Eng.*, vol. 379, p. 113741, 2021.

[6] S. Cai, Z. Wang, S. Wang, P. Perdikaris, and G. E. Karniadakis, “Physics-informed neural networks for heat transfer problems,” *J. Heat Transfer*, vol. 143, no. 6, p. 60801, 2021.

[7] ا. عرب و ع. رهی, “بررسی تحلیلی ارتعاش جانبی و پیچشی یک روتور اورهنگ با استفاده ازمدل چهار درجه آزادی جفکات,” ۱۴۰۱, تهران. لینک:https://civilica.com/doc/161112 .

[8] W. Zhou and Y. F. Xu, “Damage identification for plate structures using physics-informed

neural networks," *Mech. Syst. Signal Process.*, vol. 209, p. 111111, 2024.

[9] D. Katsikis, A. D. Muradova, and G. E. Stavroulakis, "A gentle introduction to physics-informed neural networks, with applications in static rod and beam problems," *J. Adv. Appl. Comput. Math.*, vol. 9, pp. 103–128, 2022.

[10] S. S. Rao, *Vibration of continuous systems*. John Wiley & Sons, 2019.